



## Original Articles

## IMPA2 promotes basal-like breast cancer aggressiveness by a MYC-mediated positive feedback loop



Xingyu Lei<sup>a,c,1</sup>, Ruocen Liao<sup>b,c,1</sup>, Xingyu Chen<sup>a,c</sup>, Zhenzhen Wang<sup>d</sup>, Qianhua Cao<sup>a,c</sup>, Longchang Bai<sup>a,c</sup>, Chenglong Ma<sup>a,c</sup>, Xinyue Deng<sup>b</sup>, Yihua Ma<sup>a,c</sup>, Xuebiao Wu<sup>a,e</sup>, Jun Li<sup>a,\*\*</sup>, Zhijun Dai<sup>b,\*\*\*</sup>, Chenfang Dong<sup>a,c,\*</sup>

<sup>a</sup> Department of Pathology and Pathophysiology, Department of Colorectal Surgery and Oncology, Key Laboratory of Cancer Prevention and Intervention, Ministry of Education, The Second Affiliated Hospital, Zhejiang University School of Medicine, Hangzhou, 310058, China

<sup>b</sup> Department of Breast Surgery, First Affiliated Hospital, Zhejiang University School of Medicine, Hangzhou, 310058, China

<sup>c</sup> Zhejiang Key Laboratory for Disease Proteomics, Zhejiang University School of Medicine, Hangzhou, 310058, China

<sup>d</sup> Department of Ultrasound Medicine, Cancer Center, Affiliated People's Hospital, Zhejiang Provincial People's Hospital, Hangzhou Medical College, Hangzhou, China

<sup>e</sup> Department of Pathophysiology, Gannan Medical University, Gannan, China

## ARTICLE INFO

## ABSTRACT

## Keywords:

IMPA2  
MYC  
Basal-like breast cancer (BLBC)  
Myo-inositol (MI)  
Inositol triphosphate (IP3)  
NFAT1

Basal-like breast cancer (BLBC) is the most aggressive subtype with poor prognosis; however, the mechanisms underlying aggressiveness in BLBC remain poorly understood. In this study, we showed that in contrast to other subtypes, inositol monophosphatase 2 (IMPA2) was dramatically increased in BLBC. Mechanistically, IMPA2 expression was upregulated due to copy number amplification, hypomethylation of IMPA2 promoter and MYC-mediated transcriptional activation. IMPA2 promoted MI-PI cycle and IP3 production, and IP3 then elevated intracellular  $\text{Ca}^{2+}$  concentration, leading to efficient activation of NFAT1. In turn, NFAT1 up-regulated MYC expression, thereby fulfilling a positive feedback loop that enhanced aggressiveness of BLBC cells. Knockdown of IMPA2 expression caused the inhibition of tumorigenicity and metastasis of BLBC cells in vitro and in vivo. Clinically, high IMPA2 expression was strongly correlated with large tumor size, high grade, metastasis and poor survival, indicating poor prognosis in breast cancer patients. These findings suggest that IMPA2-mediated MI-PI cycle allows crosstalk between metabolic and oncogenic pathways to promote BLBC progression.

## 1. Introduction

Breast cancer can be divided into four subtypes according to gene expression profiling: Luminal A, Luminal B, HER2, and basal-like breast cancer (BLBC) [1,2]. Among these subtypes, BLBC is often associated with larger size, higher grade and early recurrence, and usually occurs in younger and premenopausal women. In addition, about 75 % of BLBCs belong to the triple-negative breast cancer subtype, a subtype deficient in expression of ER, PR, HER2; lack of such receptors limits the use of endocrine and targeted treatments. Furthermore, BLBC has tendency to spread to brain and lung, resulting in a poor prognosis. Owing to highly aggressive nature and the absence of effective therapeutics, there is a

pressing need to elucidate its determinants of aggressiveness and identify its potential therapeutic targets [3–5].

Metabolism reprogramming as a hallmark of cancer plays a crucial role in cancer initiation and progression [6]. Myo-inositol (MI) is an important constituent of cells in animals and humans. In cell, MI can be de novo synthesized from glucose-6-phosphate (G6P) or recycled from myo-inositol-phosphatidylinositol (MI-PI) circulation, and MI from two pathway reacts with cytidine diphosphate-diacylglycerol to synthesize phosphatidylinositol (PI), which then can be metabolized into phosphatidylinositol- [4,5] bisphosphate (PIP2) and phosphatidylinositol-(3,4,5) trisphosphate (PIP3) by phosphoinositide kinases. Both PI and all phosphorylated PI-based lipids collectively form the core of a network of PI signaling pathways, modulating many cellular functions including

\* Corresponding author. Department of Pathology and Pathophysiology, Department of Colorectal Surgery and Oncology, Key Laboratory of Cancer Prevention and Intervention, Ministry of Education, The Second Affiliated Hospital, Zhejiang University School of Medicine, Hangzhou, 310058, China.

\*\* Corresponding author.

\*\*\* Corresponding author.

E-mail addresses: [2307016@zju.edu.cn](mailto:2307016@zju.edu.cn) (J. Li), [dzj0911@126.com](mailto:dzj0911@126.com) (Z. Dai), [chenfangdong@zju.edu.cn](mailto:chenfangdong@zju.edu.cn) (C. Dong).

<sup>1</sup> These authors contribute equally to this study.

## Abbreviations

IMPA2	Inositol monophosphatase 2
BLBC	Basal-like breast cancer
MI	Myo-inositol
G6P	Glucose-6-phosphate
PI	Phosphatidylinositol
PIP2	Phosphatidylinositol-[4,5] bisphosphate
IP3	Inositol triphosphate
IP6	Inositol hexaphosphate
BPD	Bipolar disorder
HD	Huntington disease
IP3R	Inositol 1, 4, 5-trisphosphate receptor
CNVs	Copy number variants
RT-qPCR	Real-time quantitative polymerase chain reaction
NFAT	Nuclear factor of activated T-cells
DMFS	Distant metastasis-free survival
OS	Overall survival
RFS	Relapse-free survival

cell proliferation, cell differentiation, apoptosis [7–9]. PIP3 is the most important second messenger in the insulin signaling cascade activation of PI3K/AKT that is crucial to cancer cell growth and survival. PIP2 is also the precursor for phospholipase C to produce inositol triphosphate (IP3), influencing the intracellular calcium signaling and cancer initiation and progression [8–10]. However, inositol hexaphosphate (IP6) is a cancer suppressor with ability of inhibition ERK-MAPK kinase cascade. These findings suggest a paradoxical role of MI in cancers [11,12].

Inositol monophosphatase 2 (IMPA2) is an enzyme that dephosphorylates inositol monophosphate into MI. Inhibition of the Inositol monophosphatase family (IMPA1 and IMPA2) results in MI depletion and a subsequent reduction of IP3-induced flux  $\text{Ca}^{2+}$  in various neurodegenerative diseases such as bipolar disorder (BPD) and Huntington disease (HD) [8,13–15]. Recent studies have shown that Inositol 1, 4, 5-trisphosphate receptor (IP3R) promotes breast cancer cells proliferation [16], survival [17] and migration [18,19], indicating a critical role in tumor progression.

In this study, we report that IMPA2 expression and MI levels are dramatically up-regulated in BLBC and predict poor prognosis in breast cancer patients. IMPA2 provides tumorigenic and metastatic advantages in BLBC through a MYC-mediated positive feedback loop.

## 2. Materials and methods

### 2.1. Plasmids and antibodies

The design of shRNA sequence targeting human IMPA2 was carried out using online tools from GPP Web Portal, then the target sequence was cloned into pLKO.1 Puro plasmid (Addgene). Human IMPA2 gene was amplified from MDA-MB468 cDNA library, and sub-cloned into pLVX-puro and pLVX-neo, respectively.

Antibodies against IMPA2, p-AKT (308), AKT, NFAT1, CnB and MYC were purchased from Abcam. Antibodies for mCherry, Lamin and  $\beta$ -actin were obtained from Sigma-Aldrich.

### 2.2. Cell culture

All cells we used in this study were obtained from the American Type Culture Collection (Manassas, VA), where the cell lines were authenticated by STR profiling before distribution. MDA-MB231, SUM159, SUM149, Hs578t and HEK293T cells were grown in Dulbecco's modified Eagle's Medium (DMEM)/F12 with 10 % FBS. HCC1954 and BT549 cells were grown in RPMI1640 plus 10 % FBS. MDA-MB468 cells were

cultured in Leibovitz's L-15 medium supplemented with 10 % FBS. For establishing stable transfectants with IMPA2 expression or knockdown of IMPA2, BLBC cells were transfected with pLVX-IMPA2 and pLKO-IMPA2sh, respectively; stable clones were selected with puromycin (300 ng/ml) for 4 weeks, respectively.

### 2.3. Quantitative real-time PCR

Total RNA was extracted from cells by AG RNAex Pro Reagent (Accurate Biology) according to the manufacturer's instructions. Reverse transcription was performed with the Evo M-MLV II Reverse Transcriptase (Accurate Biology). Real-time quantitative PCR (RT-qPCR) was performed using SYBR Green Premix Pro Taq HS qPCR Kit (Accurate Biology) following manufacturer's protocol. Gene expression level was normalized to actin level in respective samples as an internal control, and the results were representative of at least three independent experiments.

### 2.4. Methylation-specific PCR

To evaluate the methylation status of CpG sites within the IMPA2 promoter, genomic DNA was extracted from each breast cancer cell line. 1  $\mu\text{g}$  extracted DNA was bisulfite converted using the EpiTect Bisulfite Kit (Qiagen) according to the manufacturer's instructions. Methylation-specific PCR reaction was performed using  $2 \times$  EpiArt HS Taq kit (Vazyme) with the following nested primers:

Forward methylated primer: 5'-GTTATAGATTATGAAGGGACGTTG-3', Reverse methylated primer: 5'-ATCTAAATAAAACCGTACGATACCG-3', Forward unmethylated primer: 5'-GGTTATA-GATTATGAAGGGATGTTG-3', Reverse unmethylated primer: 5'-CTAAATAAAACCATAACAATACCAAC -3'

The PCR product was analyzed by gel electrophoresis, and visualized images were captured.

### 2.5. Luciferase reporter assay

The assay was performed according to the procedure described previously [20]. All experiments were performed in triplicate.

### 2.6. Chromatin immunoprecipitation (ChIP)

ChIP assays were performed as described previously [20,21]. The following primers were used for ChIP assays: 5'- TCCCGGAA-CAAAAAGCGACCG -3' and 5'- CGGCCACAGACCATGAAGGG -3' for the IMPA2 promoter. The cells were prepared to perform ChIP assay with the Imprint ChIP Kit (Sigma) according to the manufacturer's instructions and as described recently [20,21].

### 2.7. LC-MS/MS analysis of MI

Cells were trypsinized and counted. Following centrifugation, cells were washed with PBS twice. The pellet was resuspended in distilled water, rapidly extracted (within 20–30 s) and snap frozen in liquid nitrogen. The substrates were centrifuged at 14 000 rpm for 10 min at 4 °C, and then the supernatants were stored frozen at –80 °C until analysis.

For the quantitative method, the LC-MS/MS system was composed of a Waters Xevo TQ tandem quadrupole mass spectrometer (Waters Micromass MS Technologies, Manchester, UK) coupled with a Waters ACQUITY UPLC system autosampler. All analytes were determined on an Agilent Polaris Amide (2.0  $\times$  100 mm, 5  $\mu\text{m}$ )-C8 column. The mobile phase for pump A consisted of acetone/acetonitrile (50:50, v/v), while the mobile phase for pump B was 5 mM ammonium acetate. The LC pumps were programmed to deliver 85 % pump A and 15 % pump B at a flow rate of 0.3 mL/min. The sample injection volume was 3  $\mu\text{L}$ , and the cycle time was 45 min/injection. The wash solvent for this LC system was also acetonitrile/water (50:50, v/v). The mass spectrometer with

electrospray ionization (ESI) source was operated in negative mode. The optimized desolvation temperature was 250 °C. The capillary voltage was set at 3000 V. Cone and desolvation gas flows were set to 90 and 900 L/h, respectively. Quantification was performed using selected reaction monitoring (SRM) of the transitions of *m/z* 178.8 → 86.4 for myo-inositol. The optimized collision voltages was 70 V. Standard curves were prepared at concentrations of 25, 50, 125, 250, 500, 1250, 1750, 2500 pg/mL for standard myo-inositol (Sigma). Samples were diluted in water to ensure their concentrations fell within the standard curve range.

### 2.8. *Ca<sup>2+</sup>* imaging

Cells plated on glass bottom cell culture dishes were loaded with the calcium-sensitive fluorescent dye Fluo-4/AM (4 mM; Invitrogen) in Krebs-Ringer Bicarbonate HEPES Buffer containing 0.02 % pluronic acid (Sigma) for 1 h at 37 °C. ATP (Sigma) and Histamine (Sangon biotech) were applied at concentrations 10 μM. EGTA (Sigma-Aldrich) was used to chelate extracellular Ca<sup>2+</sup>. Fluorescence was measured by an Olympus Confocal Laser Scanning Microscope (DU-897D-CSO) using MetaMorph software. Serial scanning was performed at 488/530 nm excitation/emission wavelengths at 3 s intervals. Fluorescence intensity changes (F%) were shown as the percentage of baseline fluorescence.

### 2.9. Immunostaining

Experiments were performed as described previously. Cells grown on chamber slides were fixed for 15 min with 4 % paraformaldehyde, permeabilized for 10 min in phosphate-buffered saline (PBS) containing 0.2 % TritonX-100, blocked for 1 h with 1 % BSA and 0.5 % goat serum in PBS, and then incubated with primary antibodies at 4 °C overnight. Secondary antibodies used were Texas red-conjugated goat anti-mouse or FITC-conjugated goat anti-rabbit. fluorescence was measured using an Olympus Confocal Laser Scanning Microscope (OLYMPUS IX83-FV3000-OSR).

### 2.10. IP3 assay

Cells were grown on 10 cm cell-culture dishes for 90 % confluence, and then cells were washed and lysed. Cell lysates were collected and centrifuged at 12,000 rpm to acquire the supernatants. The level of IP3 in supernatant was measured using an ELISA kit (Abcam) according to the manufacturer's instruction.

### 2.11. Colony formation assay

Colony formation assay was performed using double-layer soft agar in 24-well plates with a bottom layer of 0.7 % agar and a top layer of 0.35 % agar. Cells were seeded in 24-well plates and cultured at 37 °C for 15–20 days, and the colonies were stained and counted.

### 2.12. Migration and invasion assays

Migration and invasion assays were carried out as described previously [22]. All experiments were performed at least twice in triplicate. Statistical analysis was performed using the Student's *t*-test; a p-value of <0.05 was considered significant.

### 2.13. Tumorigenesis assay and lung metastasis model

Animal experiments were performed according to the approved procedures by the Institutional Animal Care and Use Committee at Zhejiang University. To test the effect of IMPA2 on in vivo tumorigenesis, female SCID mice (8 weeks old) were injected with  $1 \times 10^6$  exogenous IMPA2 knockdown cells in the left flank and vector control cells in the right flank. Tumor formation and growth were monitored every 2

days for 30 days, and tumor size and weight were determined. To evaluate the effect of IMPA2 on tumor lung metastasis, SCID mice were injected via tail vein with MDA-MB231 cells ( $1 \times 10^6$  cells/mouse) with stable empty vector or knockdown of IMPA2 expression (6 mice/group). After 4 weeks, lung metastasis was examined by an IVIS-100 imagining system (Xenogen). Lung metastatic nodules were analyzed in paraffin-embedded sections stained with hematoxylin and eosin. Data analyses were performed using the Student's *t*-test; a p-value <0.05 was considered significant.

### 2.14. Statistical analysis

Results are expressed as mean ± SD or SEM as indicated. Comparisons were made by the two-tailed Student's *t*-test or one-way ANOVA. Correlations were analyzed by Pearson's correlation method and Spearman's rank correlation test. Survival curves were performed using the Kaplan-Meier method, and differences were analyzed by the log-rank test. In all statistical tests, P < 0.05 was considered statistically significant.

## 3. Results

### 3.1. IMPA2 is up-regulated in BLBC subtype

We have showed the critical roles of FPB1, AKR1B1, UGT8, ABAT, PLSCR1 and B3GNT5 in BLBC aggressiveness [22–27]. In order to further identify the other enzymes required for BLBC, we systematically analyzed available breast cancer expression datasets (GSE25066, NKI295, METABRIC, TCGA) [28–30]. In addition to some metabolic genes previously reported, such as UGT8 and FPB1, IMPA2 mRNA expression was notably higher in BLBC (Fig. 1A and Supplementary Fig. S1A). In line with mRNA expression, IMPA2 protein expression was significantly elevated in TCGA proteomic dataset (Fig. 1B) [31]. To verify this observation, we examined fourteen cases of luminal subtype and twelve cases of the triple-negative subtype that has a significant overlap with BLBC, showing that IMPA2 was remarkably up-regulated in triple-negative subtype (Fig. 1C and Supplementary Fig. S1B). To further explore the association of IMPA2 mRNA expression with basal subtype, we also analyzed IMPA2 mRNA expression in GSE12777 and GSE10890 breast cancer cell line datasets [32,33]. Consistently, IMPA2 mRNA expression was upregulated in basal subtype cell lines (Fig. 1D). To confirm these results, we tested a representative panel of breast cancer cell lines that contained five luminal and five BLBC cell lines by either semiquantitative RT-PCR or quantitative real-time PCR, showing that IMPA2 mRNA expression was also much higher in BLBC cells than in luminal cells (Fig. 1E and F). We further examined IMPA2 protein expression by western blotting. Strikingly, elevated IMPA2 protein level was observed in BLBC cells (Fig. 1G). We also analyzed the expression level of IMPA2 in normal breast tissues and luminal breast cancer tissues, showing that there was no significant difference of IMPA2 expression between luminal subtype and normal tissues (Supplementary Figs. S1C and D). Together, our data indicate that IMPA2 overexpression is tightly associated with BLBC.

### 3.2. IMPA2 copy number amplification and hypomethylation of IMPA2 promoter contribute to the overexpression of IMPA2 in BLBC

Copy Number Variants (CNVs) has been found to be abundant in human cancers [34]. To explore whether IMPA2 expression was affected by CNVs, we analyzed the copy number alterations of breast cancer in TCGA, METABRIC and CCLE datasets. We observed that cases with IMPA2 amplification had remarkably higher IMPA2 mRNA expression than those with no amplification, supporting the notion that high IMPA2 level might correlate with IMPA2 copy number amplification (Fig. 2A and B and Supplementary Fig. S2A). Subsequently, we also analyzed the copy number alterations in different subtypes of breast cancer tissues,

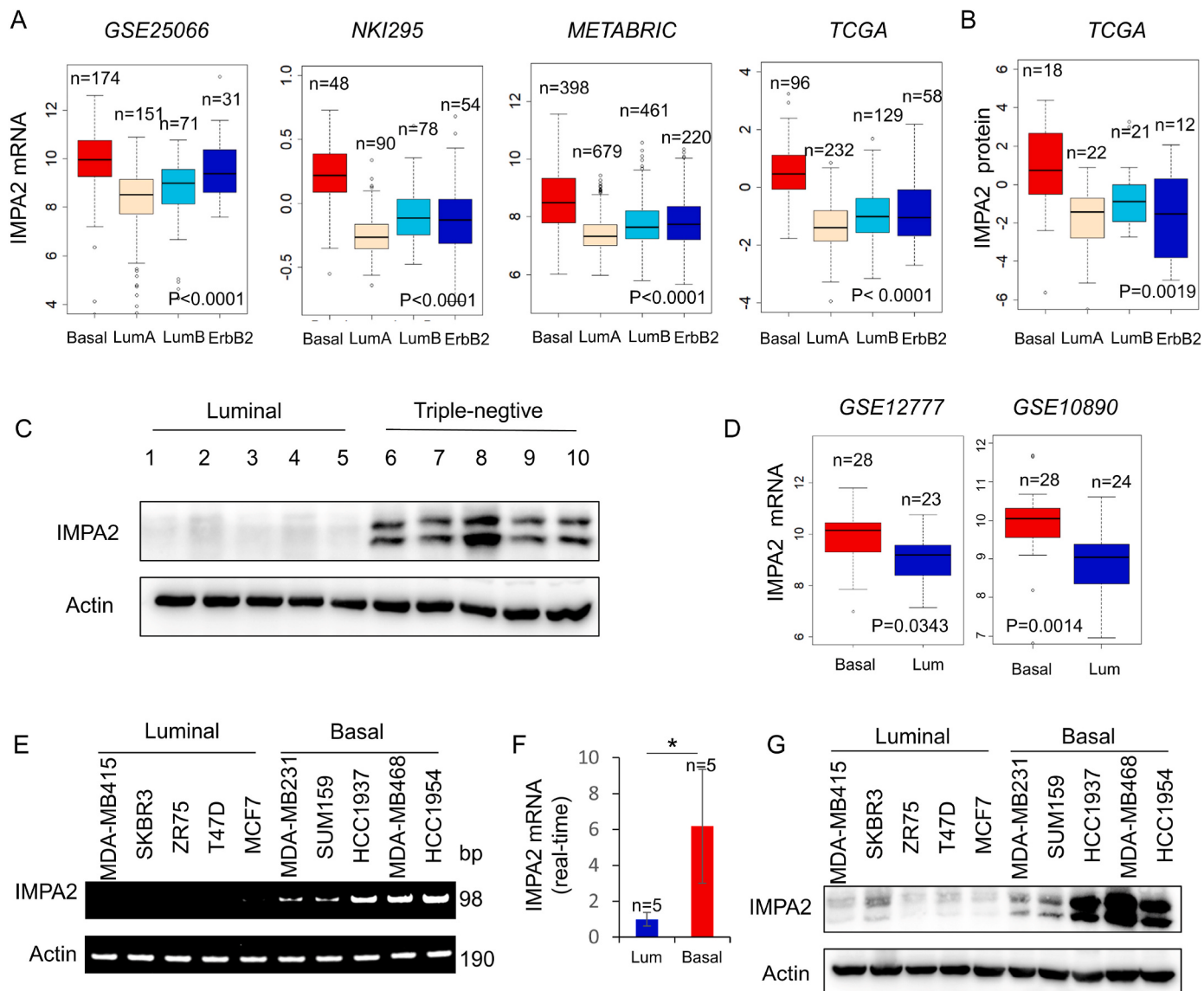


**Fig. 1.** Elevated IMPA2 expression highly correlates with BLBC. (A) Box-plots indicated IMPA2 mRNA expression in four different subtypes of breast cancer from four datasets (GSE25066, NKI295, METABRIC and TCGA). (B) Box-plots indicated IMPA2 protein expression in different subtypes of breast cancer from the TCGA dataset. (C) Expression of IMPA2 was examined by Western blotting in tumor samples from five cases of luminal and five cases of triple-negative breast cancers. (D) Box plots indicated IMPA2 mRNA expression in luminal and BLBC cell lines from GSE12777 and GSE10890 datasets. (E, F) Expression of IMPA2 mRNA was analyzed by either semi-quantitative RT-PCR (E) or quantitative real-time PCR (F) in breast cancer cell lines. (G) Expression of IMPA2 was examined by Western blotting in breast cancer cell lines. Data are shown as mean  $\pm$  SD based on three independent experiments. \*, P < 0.05 by Student's t-test.

finding that IMPA2 copy number amplification predominantly existed in BLBC subtype (Fig. 2C-F and Supplementary Figs. S2B and C). These data suggest that IMPA2 copy number amplification is positively correlated with IMPA2 overexpression and BLBC subtype.

Since many tumors with high expression of IMPA2 did not have copy number amplification of IMPA2, other factors might associate with this event. DNA methylation, as an important regulator of gene transcription, plays a crucial role in cancer progression [35]. To determine the effect of DNA methylation on IMPA2 expression in breast cancer, we then analyzed methylation and expression of IMPA2 from two datasets (TCGA and GSE44837). The correlation between IMPA2 expression and IMPA2 methylation was analyzed by gene expression microarray and 450K Infinium microarray. As expected, the methylation of IMPA2 promoter regions in BLBC had a significant decrease compared with other subtypes (Fig. 2I and J and Supplementary Fig. S2D). In addition, IMPA2 mRNA expression was negatively correlated with IMPA2 promoter methylation (Fig. 2K-L and Supplementary Fig. S2E).

Subsequently, we also performed methylation-specific PCR test, showing that the IMPA2 promoter region in BLBC cell lines had an apparent reduction in methylation compared with that in luminal breast cancer cell lines (Fig. 2M). These data strongly indicate that hypomethylation of IMPA2 promoter is another important reason for IMPA2 overexpression.

### 3.3. IMPA2 is a direct target of MYC

Given that many tumors with high expression of IMPA2 did not have copy number amplification or hypomethylation of IMPA2, other factors might involve this event. Coexpression analysis of IMPA2 with other molecules in two large gene expression datasets showed that IMPA2 expression positively correlated with MYC expression (Fig. 3A). We then analyzed MYC expression in different subtypes of breast cancer, showing that similar to IMPA2, MYC was dramatically up-regulated in BLBC in these gene expression datasets (Fig. 3B). To investigate the causal

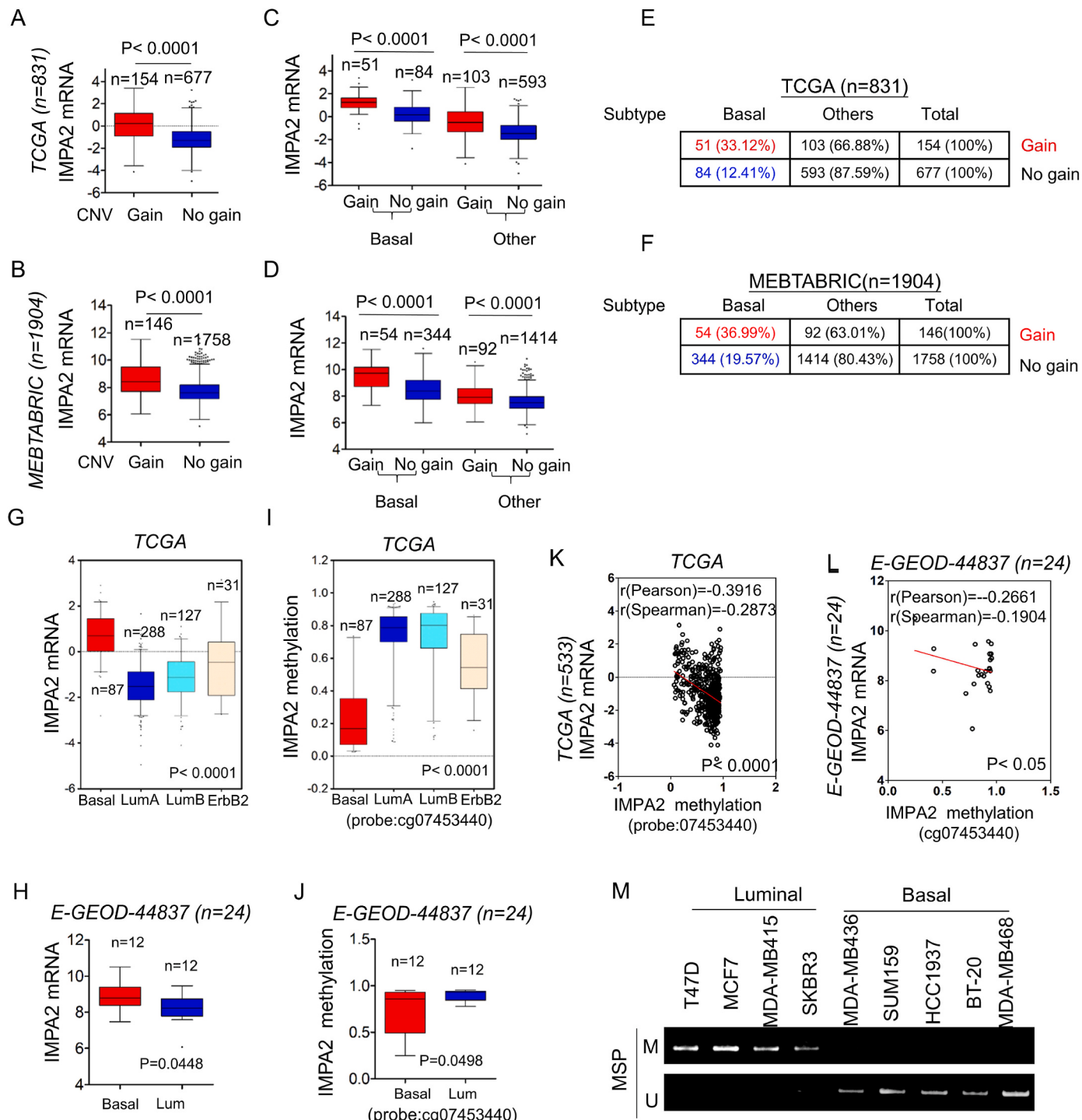
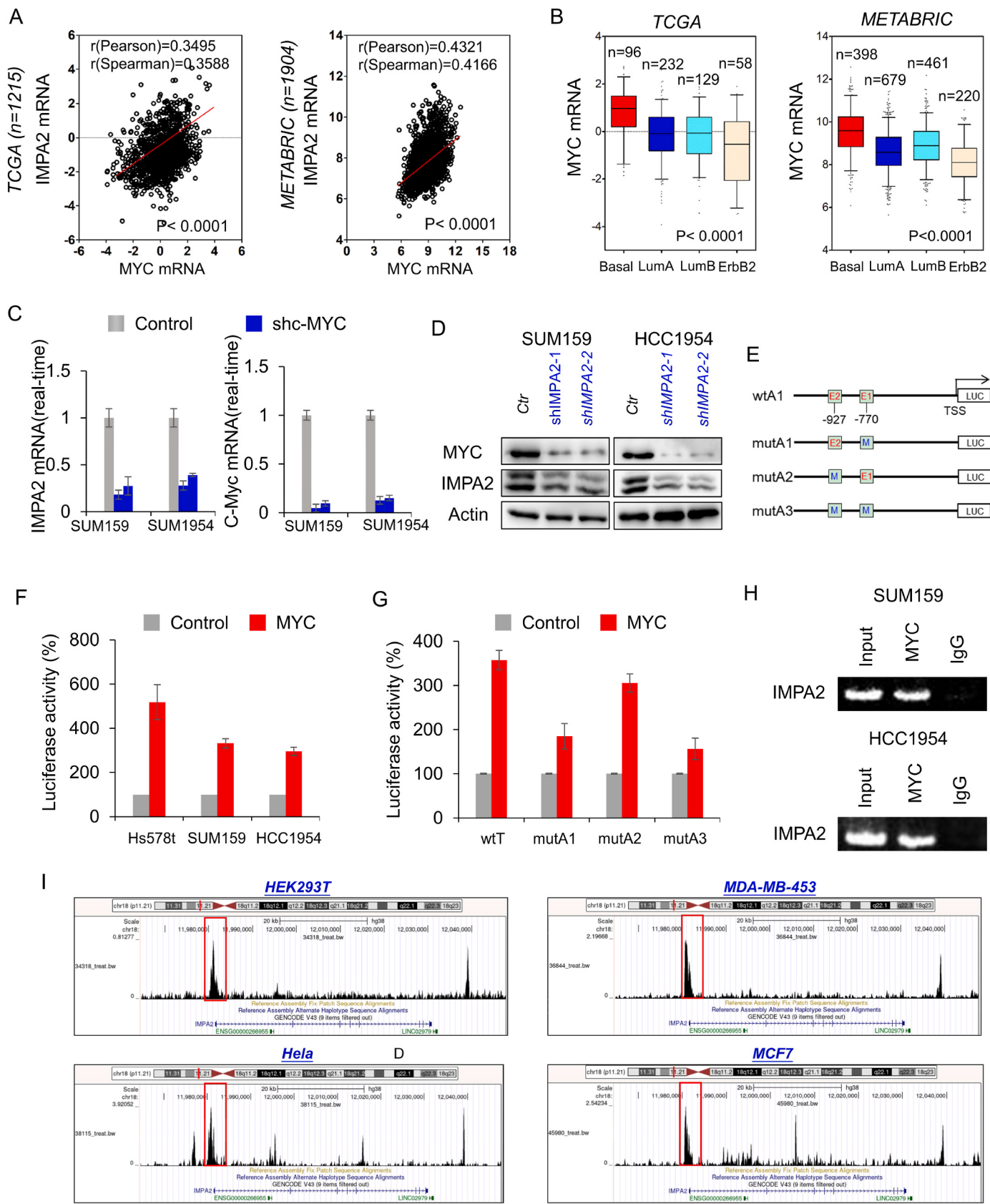


**Fig. 2.** IMPA2 overexpression associates with its copy number amplification and promoter hypomethylation. (A, B) Box-plots indicated the correlation of IMPA2 mRNA expression with its copy number variants status (gain and no gain) in breast cancer from the TCGA dataset (A) and MEBTABRIC dataset (B). (C, D) Box-plots showed the association of IMPA2 mRNA level with copy number variants (gain and no gain) in different subtypes of breast cancer from the TCGA dataset (C) and MEBTABRIC dataset (D). (E, F) Analysis of the correlation of IMPA2 mRNA expression with its copy number status (gain or no gain) in breast cancer from the TCGA dataset (E) and MEBTABRIC dataset (F). (G, H) Box-plots indicated IMPA2 mRNA expression in different subtypes of breast cancer (TGCA dataset) (G) and breast cancer cell lines (GSE44837 dataset) (H). (I, J) Box-plots indicated IMPA2 promoter methylation in different subtypes of breast cancer (TGCA dataset) (I) and breast cancer cell lines (GSE44837 dataset) (J). (K, L) Analysis of the mRNA expression and methylation of IMPA2 from the TCGA dataset (K) and GSE44837 dataset (L). The relative level of IMPA2 mRNA was plotted against that of IMPA2 methylation. Comparisons are made using the two-tailed Student's t-test. (M) IMPA2 promoter methylation was analyzed by methylation-specific PCR.



(caption on next page)

**Fig. 3.** IMPA2 positively correlates with MYC and is a direct transcriptional target of MYC (A) Analysis of the mRNA expression of IMPA2 and MYC from the TCGA dataset and METABRIC dataset. The relative level of IMPA2 mRNA was plotted against that of MYC mRNA. Comparisons are made using the two-tailed Student's t-test. (B) Box-plots indicated MYC mRNA expression in four different subtypes of breast cancer from the TCGA dataset and METABRIC dataset. (C) Expression of IMPA2 and MYC was analyzed by quantitative RT-PCR in SUM159 and HCC1954 cells with empty vector or knockdown of IMPA2 expression. Data are shown as mean  $\pm$  SD based on three independent experiments. \*, P < 0.01 by Student's t-test. (D) Expression of IMPA2 and MYC was examined by Western blotting in SUM159 and HCC1954 cells with empty vector or knockdown of IMPA2 expression. (E) Schematic diagram showing positions of potential MYC-binding E-boxes in IMPA2 promoter and IMPA2 promoter luciferase (LUC) constructs used. (F) IMPA2 promoter luciferase construct (wtA) was coexpressed with empty vector or MYC in Hs-578t, SUM159 and HCC1954 cells respectively. After 48 h, luciferase activities were determined and normalized (mean  $\pm$  SD in three separate experiments). (G) IMPA2 promoter luciferase construct (wtA1) as well as its E-box mutants (mutA1, mutA2, and mutA3) were coexpressed with empty vector or MYC in SUM159 cells. Luciferase activities were determined and normalized (mean  $\pm$  SD in three separate experiments). (H) ChIP analysis for binding of MYC to the IMPA2 promoter in SUM159 and HCC1954 cells. (I) ChIP-seq analysis of read distribution and genomic localization of MYC around the promoter of IMPA2 gene.

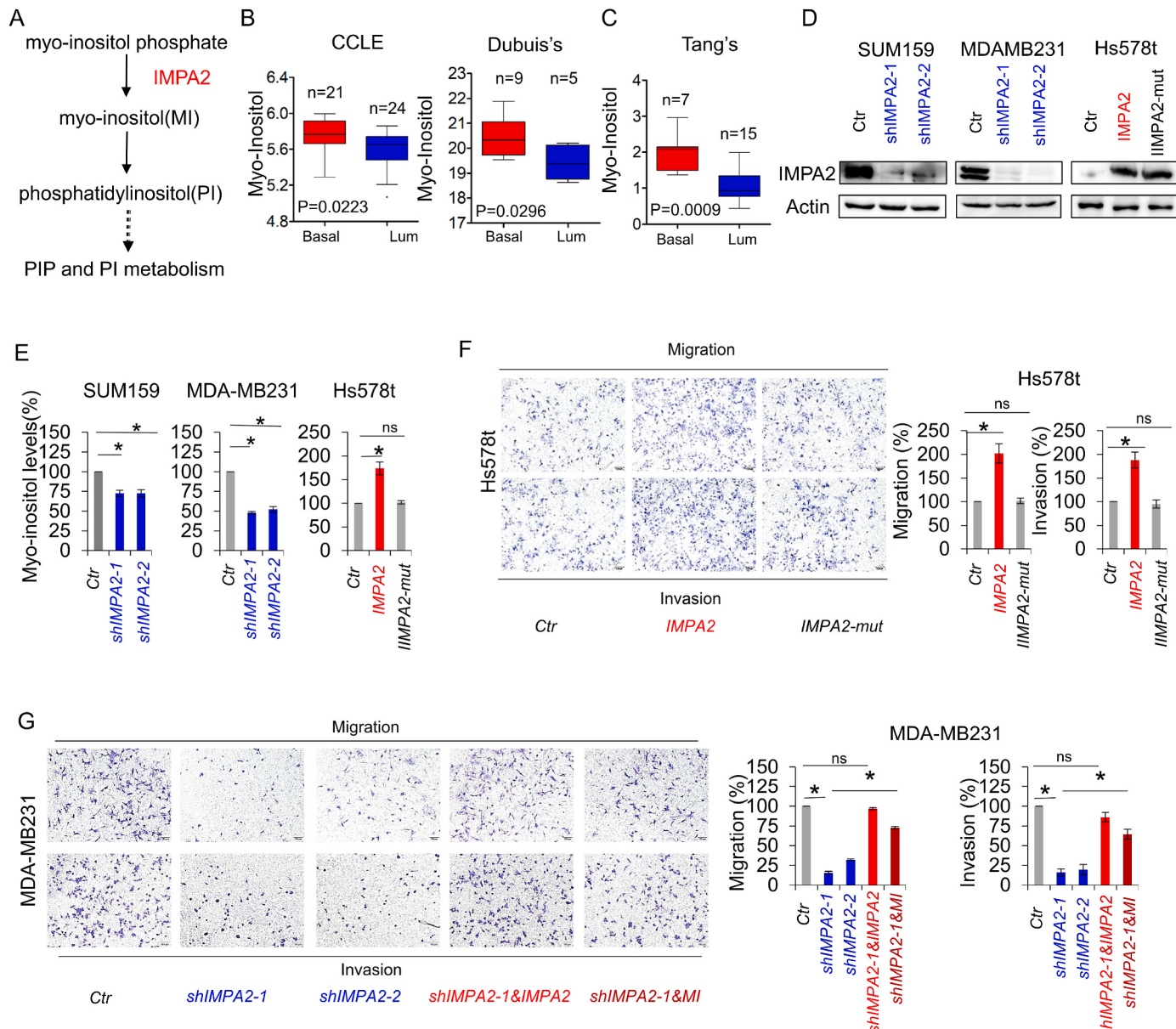


**Fig. 4.** IMPA2 promotes intracellular MI levels, migration and invasion of breast cancer cells. (A) MI metabolic pathway. (B, C) MI level was analyzed in BLBC versus luminal from three metabolomics datasets (CCLE, Dubuis's and Tang's metabolomics dataset). (D) Stable transfectants with empty vector or knockdown of IMPA2 expression were established in SUM159 and MDA-MB231 cells, and stable clones with empty vector, IMPA2 or IMPA2-mut expression were also generated in Hs578t cells. IMPA2 expression in these cells was analyzed by Western blotting. (E) MI Level was examined by LC-MS/MS in SUM159 and MDA-MB231 cells with stable empty vector or knockdown of IMPA2 expression, as well as Hs578t cells with stable empty vector, IMPA2 or IMPA2-mut expression. (F, G) Migratory ability and invasiveness of Hs578t cells with stable empty vector, IMPA2 or IMPA2-mut expression (F) and MDA-MB231 with stable empty vector or knockdown of IMPA2 expression as well as shIMPA2-expressing MDA-MB231 with IMPA2 re-expression or MI (50  $\mu$ M) treatment (G). Scale bar = 100  $\mu$ m (right). The percentage of migratory and invasive cells is shown in the bar graph (mean  $\pm$  SD of three separate experiments). \*p < 0.01 by Student's t-test.

relationship between IMPA2 and MYC, we generated a stable clones with empty vector or knockdown of MYC expression in SUM159, HCC1954 cells, and also created stable transfectants with empty vector, MYC expression in Hs578t cells. We found that knockdown of MYC expression resulted in a remarkable downregulation, whereas exogenous MYC expression caused a significant upregulation of IMPA2 expression (Fig. 3C and D *Supplementary Figs. S3A and B*). These results indicate that MYC, as a transcriptional activator, may induce IMPA2 expression through transcriptional regulation.

Having identified their tight association and immediate induction of IMPA2 expression by MYC, we next determined whether IMPA2 expression was regulated directly by MYC. We observed that it contains five putative MYC-binding E-boxes (CACGTG, CACATG, CATGTG or CACGCG) from -1590 bp to the transcription start site (TSS) (Fig. 3E). We cloned the human IMPA2 promoter and generated several deletion mutants of promoter-luciferase constructs based on the location of these E-boxes, including wtA (-1590 bp), wtA1 (-1020 bp) and wtA2 (-620 bp) (*Supplementary Fig. S3C*). By expressing the wtA in Hs578t, SUM159 and HCC1954 cells, MYC significantly promoted IMPA2 promoter luciferase activity (Fig. 3F). The wtA1 without the region between -1590 and -1020 bp still maintained high reporter activity induced by MYC, whereas the wtA2 (-620 bp) lost the activity to respond to MYC expression (*Supplementary Fig. S3D*). Thus, the region between -1020 and -620 bp might be important for MYC-mediated IMPA2 activation. To pinpoint the exact binding E-boxes, we introduced point mutations into E1 and/or E2. Mutation in E2 (mutA2) only weakly reduced, whereas mutation in either E1 (mutA1) or both E-boxes (mutA3) almost completely abolished, MYC-mediated activation of the IMPA2 promoter luciferase (Fig. 3G), suggesting that MYC activates the IMPA2 promoter in an E-box-dependent fashion and that the E-box at -770 bp is required for MYC-induced transcriptional activation. To determine whether MYC targets IMPA2 directly, we performed chromatin immunoprecipitation (ChIP) assays in HCC1954, and SUM159 cells with MYC overexpression. The results showed that MYC directly bound to the IMPA2 promoter (Fig. 3H), indicating that IMPA2 is a direct target of MYC. Consistently, multiple MYC-specific chromatin immunoprecipitation (ChIP)-seq analysis showed that MYC was observed to be highly enriched in the promoter of IMPA2 in HEK293T, Hela, MDA-MB453 and MCF7 cells (Fig. 3I).

#### 3.4. IMPA2 expression increases MI levels and promotes breast cancer cell migration and invasion

We first analyzed the association of MI, a direct product of IMPA2, with BLBC in previous metabolomics datasets (CCLE, Dubuis and Tang's metabolomics datasets) and found MI level was much higher in BLBC cells and tumor samples (Fig. 4B and C) [36,37]. To further explore the association of IMPA2 with MI, we generated a stable clones with empty vector or knockdown of IMPA2 expression in MDA-MB231, MDA-MB468 and SUM159 cells, and also created stable transfectants with empty vector, IMPA2 expression or IMPA2-D104 N with a loss of enzymatic activity in BT-549 and Hs578t cells [38]. We found that knockdown of IMPA2 expression resulted in a remarkable decrease, whereas exogenous IMPA2 expression but not IMPA2 D104 N caused a significant increase in MI level (Fig. 4D and E and *Supplementary Figs. 4A and B*), indicating that IMPA2 and its enzymatic activity are required for MI production in breast cancer cells. We also tested the effect of IMPA2 expression and MI on breast cancer migration and invasion. Knockdown IMPA2 markedly inhibited the migration and invasion of MDA-MB231 and SUM159 cells in vitro, whereas IMPA2 expression but not IMPA2 D104 N dramatically promoted the migration and invasion of BT549 and Hs-578t cells, indicating that IMPA2 promotes breast cancer cells the migration and invasion in an enzyme activity-dependent manner (Fig. F and *Supplementary Figs. S4C-E*). To test if MI is required IMPA2 function, we added MI in culture medium or expressed IMPA2 in MDA-MB231 cells with stable knockdown of IMPA2, showing

that both MI and IMPA2 could rescue MDA-MB231 migratory and invasive ability (Fig. 4G). These data support a critical role of MI in IMPA2-mediated acquisition of migratory and invasive ability in breast cancer cells.

#### 3.5. IMPA2 expression upregulates intracellular $\text{Ca}^{2+}$ concentration

MI can be metabolized into phosphatidylinositol (PI), and PI can be further phosphorylated to phosphatidylinositol-4-phosphate (PIP), phosphatidylinositol-biphosphate (PIP2) and phosphatidylinositol-trisphosphate (PIP3) (Fig. 5A). In cancer, PI can regulate PI3K/AKT activation by PIP3 or  $\text{Ca}^{2+}$  concentration by IP3 to promote cancer cells proliferation, migration and survival. We first detected the level of p-AKT (308) in MDA-MB231 and SUM159 cells with stable empty vector or knockdown of IMPA2 expression, showing that no obvious change was observed (Fig. 5B). In neurons, MI pool can directly regulate IP3 level. To assess the association of IMPA2 expression with IP3 level and  $\text{Ca}^{2+}$  concentration, we used an IP3 ELISA kit to test the relationship between IMPA2 expression and IP3 level. As expected, knockdown of IMPA2 expression significantly decreased the IP3 level in MDA-MB231 and SUM159 cells (Fig. 5C). Subsequently, we examined the  $\text{Ca}^{2+}$  flux in MDA-MB231 and SUM159 cells with stable empty vector or knockdown of IMPA2 expression. Remarkably, knockdown of IMPA2 expression had a lower  $\text{Ca}^{2+}$  flux (Fig. 5D-K and *Supplementary Figs. S5A-H*). We also tested  $\text{Ca}^{2+}$  flux in Hs578t with stable empty vector or IMPA2 expression. Consistently, IMPA2 expression caused a significant increase of  $\text{Ca}^{2+}$  flux (Fig. 5L-O). These data suggest that IMPA2-mediated increase of IP3 level elevates  $\text{Ca}^{2+}$  concentration in breast cancer cells.

#### 3.6. IMPA2 enhances NFAT1 activation and elevates MYC expression

Nuclear factor of activated T-cells (NFAT) is the direct downstream effector of  $\text{Ca}^{2+}$  oscillations [39,40]. To test the association of IMPA2-mediated IP3/ $\text{Ca}^{2+}$  changes with NFAT1. We determined the effect of IMPA2 on nuclear translocation of NFAT1. Our results showed that knockdown of IMPA2 expression led to a significant decrease in translocation of NFAT1 in MDA-MB231 and SUM159 cells as detected both by immunostaining confocal analysis and Western blotting analysis (Fig. 6A, C), whereas IMPA2 expression caused an apparent increase in translocation of NFAT1 in Hs578t (Fig. 6B, D). To verify that IMPA2 promotes nuclear translocation of NFAT1 through IP3R-mediated calcium signaling, we added 2-APB, a IP3R inhibitor, in Hs-578t cells with stable IMPA2 expression, and then detected its effect on NFAT1, showing that 2-APB could effectively inhibit IMPA2-mediated nuclear translocation of NFAT1 (*Supplementary Figs. S6A and B*). Together, these data support that IMPA2 functions mainly via  $\text{Ca}^{2+}$ -mediated NFAT1 signaling.

It has been reported that NFAT1 is a direct transcriptional activator for MYC [41–43]. To further test the association of IMPA2-mediated NFAT1 activation with MYC. We first treated SUM159 and HCC1954 cells with TGF- $\beta$  that is an activator of NFAT1 and MYC, or with stable knockdown of NFAT1 expression. Western blotting data showed that TGF- $\beta$  up-regulated NFAT1 and MYC expression, whereas knockdown of NFAT1 blocked this upregulation in MYC (Fig. 6E). Next, we detected SUM159 and HCC1954 cells with stable empty vector or knockdown of IMPA2 expression and Hs578t with stable empty vector or IMPA2 expression by Western blotting analysis, showing that knockdown of IMPA2 expression led to a significant decrease, whereas IMPA2 expression caused an apparent increase in MYC expression (Fig. 6F and G). Together, IMPA2-mediated NFAT1 activation promotes MYC expression, forming a positive feedback loop that regulates the functions of breast cancer cells (Fig. 6H).

#### 3.7. IMPA2 promotes tumorigenicity of breast cancer

Given the strong association of IMPA2-mediated metabolic alteration

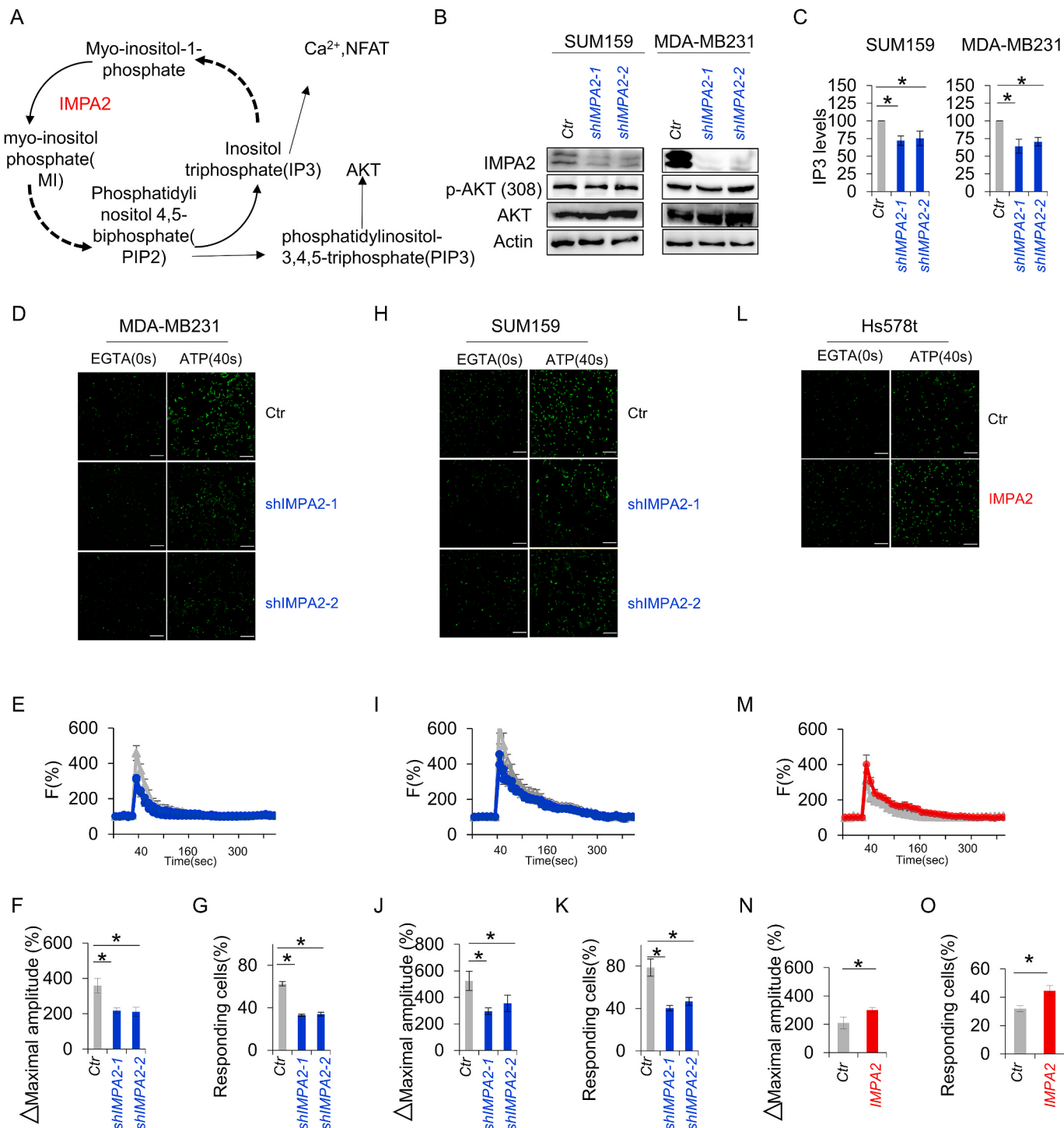


**Fig. 5.** IMPA2 expression increases intracellular IP3 levels and upregulates intracellular  $\text{Ca}^{2+}$  concentration. (A) Schematic of MI-PI cycle and PI signaling. (B) Expression of IMPA2, p-AKT (308), AKT was analyzed by Western blotting in SUM159 and MDA-MB231 cells with stable empty vector or knockdown of IMPA2 expression. (C) IP3 level was examined by ELISA in SUM159 and MDA-MB231 cells with stable empty vector or knockdown of IMPA2 expression. (D–H)  $\text{Ca}^{2+}$  signals were measured in Fura-4-AM-loaded SUM159 cells (D–G) and MDA-MB231 cells (H–K) transfected with stable empty vector or knockdown of IMPA2 expression as well as Hs578t cells with stable empty vector or IMPA2 expression (L–O). EGTA (3 mM) was added to chelate extracellular  $\text{Ca}^{2+}$ , and after 35s ATP (10  $\mu\text{M}$ ) was added to activate IP3-mediated  $\text{Ca}^{2+}$  release. Representative fluorescence images (D, H, L) and Calcium imaging traces (E, I, M) were shown. Scale bar = 300  $\mu\text{m}$  (right). Percentage of maximal peak amplitude (F, J, N) and responding cells (G, K, O) also were calculated (mean  $\pm$  SD of three separate experiments). \*p < 0.01 by Student's t-test.

with oncogenic signaling in BLBC, we first examined colony-formation by soft agar assay. Knockdown of IMPA2 expression caused a remarkable decrease of colony-formation in SUM159, MDA-MB231, MDA-MB468, MDA-MB435 and HCC1954 cells (Fig. 7A), whereas IMPA2

expression led to an apparent increase of colonies in BT-549 and Hs578t cells (Fig. 7B). To investigate the effect of IMPA2 on luminal breast cancer cells. We examined colony-formation and proliferation ability, showing that IMPA2 overexpression didn't significantly affect cell

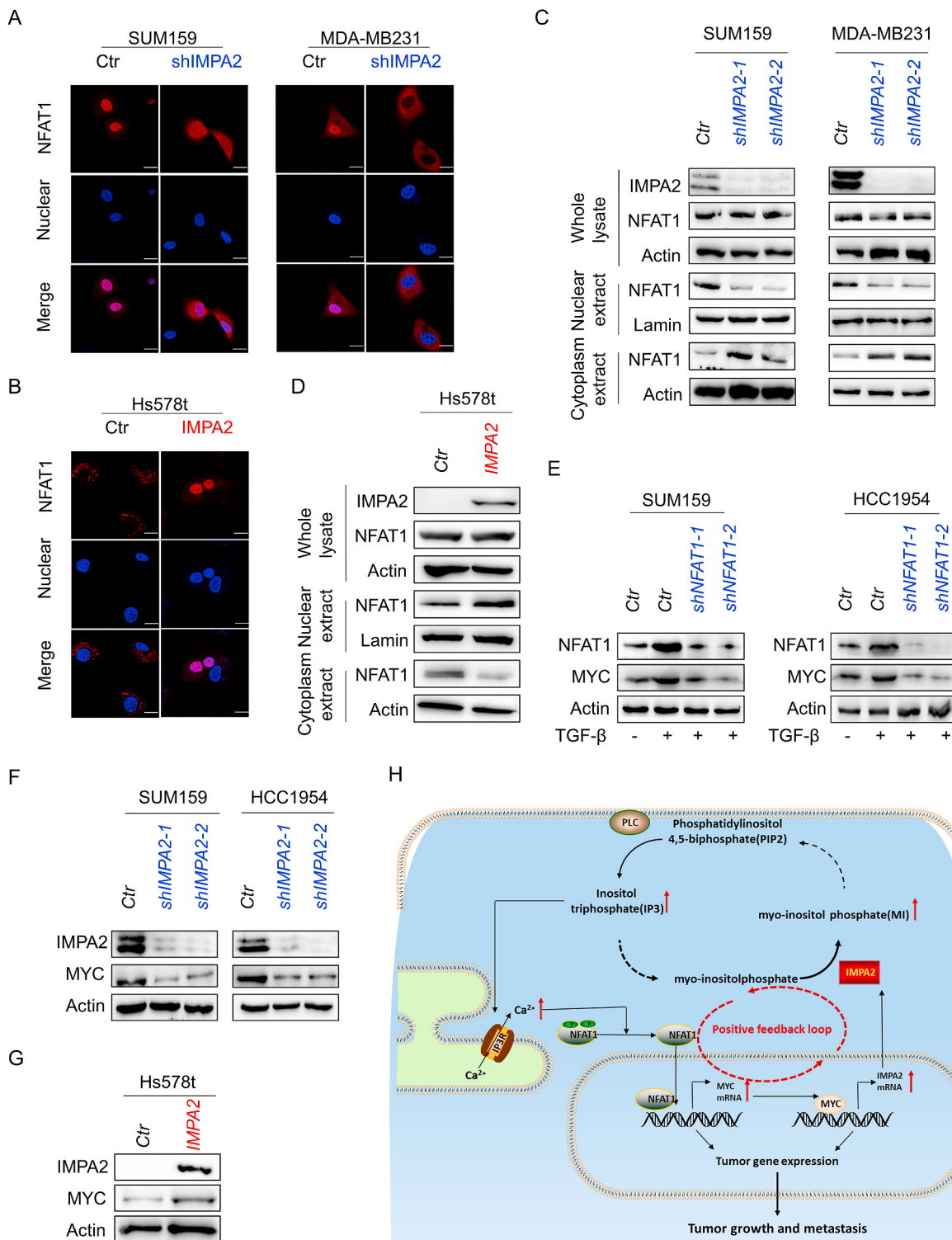


**Fig. 6.** IMPA2 promotes NFAT1-MYC axis activation. (A, B) Nuclear translocation of NFAT1 was measured by immunofluorescent staining in SUM159 and MDA-MB231 cells (A) with stable empty vector or knockdown of IMPA2 expression as well as Hs578t cells (B) with stable empty vector or IMPA2 expression. Scale bar = 10  $\mu$ m (right). (C, D) Expression of NFAT1 and IMPA was analyzed by Western blotting in MDA-MB231 and SUM159 cells (C) with stable empty vector or knockdown of IMPA2 expression as well as Hs578t cells (D) with stable empty vector or IMPA2 expression. (E) Expression of NFAT1 and MYC was analyzed by Western blotting in SUM159 and HCC1954 with stable empty vector, knockdown of NFAT1 expression or/and TGF- $\beta$  (10 ng/ $\mu$ l) treatment (24h). (F, G) Expression of IMPA2 and MYC was analyzed by Western blotting in SUM159 and HCC1954 cells (F) with stable empty vector or knockdown of IMPA2 expression as well as Hs578t cells (G) with stable empty vector or IMPA2 expression. (H) A proposed model to illustrate the regulation of IMPA2 by a MYC-mediated positive feedback loop, leading to tumor growth and metastasis.

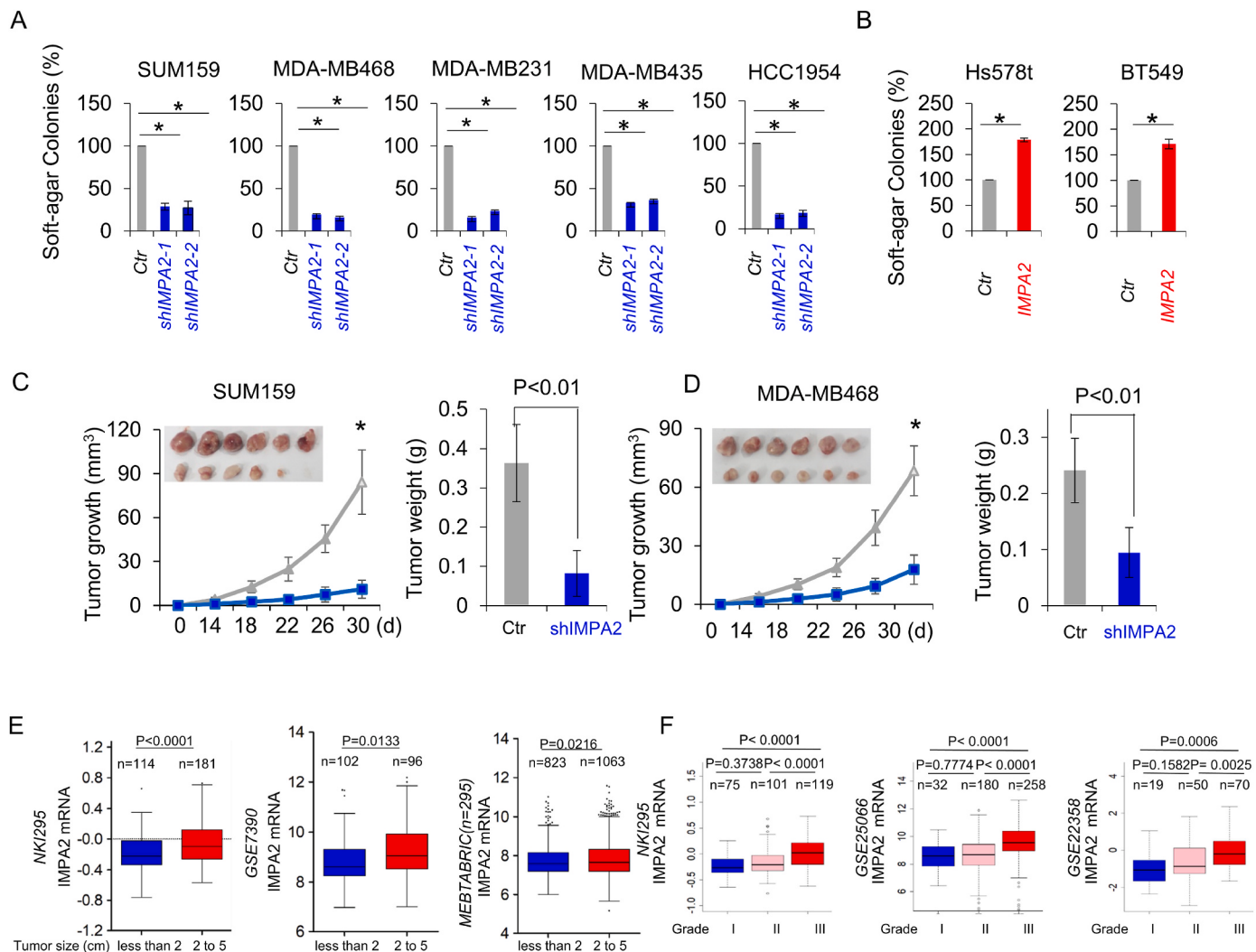


**Fig. 7.** Knockdown of IMPA2 expression inhibits tumorigenicity in vitro and in vivo. (A, B) Soft-agar assay was performed using SUM159, MDA-MB468, MDA-MB231, MDA-MB435 and HCC1954 cells with stable empty vector or knockdown of IMPA2 expression (A) as well as Hs578t and BT549 cells with stable empty vector or IMPA2 expression (B). Data are presented as a percentage of empty vector cell lines (mean  $\pm$  SD in three separate experiments). (C, D) SUM159 cells (C) and MDA-MB468 cells (D) with stable empty vector or knockdown of IMPA2 expression were injected into the mammary fat pad of SCID mice. The growth of tumors was examined every 4 d. On 30 day, mice were sacrificed and tumor weights were recorded. Data are shown as mean  $\pm$  SEM from six mice. \*, P < 0.001. (E) Box-plots indicated IMPA2 expression in different tumor sizes of breast cancer from three datasets (NKI295, GSE7390 and MEBTABRIC). Comparisons are made using the two-tailed Student's t-test. (F) Box-plots indicated IMPA2 expression in different histological grades of breast cancer from three datasets (NKI295, GSE25066 and GSE22358). Comparisons between two groups are made using the two-tailed Student's t-test.

proliferation and colony-formation in two luminal breast cancer cells ([Supplementary Figs. S7A and B](#)). To explore the effect of IMPA2 on cell cycle, we treated cells with propidium iodide (PI), showing knockdown of IMPA2 expression led to an increase in G2/M phase arrest and a decrease in G0/G1 and S phases ([Supplementary Fig. S7C](#)).

We then tested the tumorigenicity in vivo by tumor xenograft experiments in female SCID mice. Compared with control cell, SUM159 and MDA-MB468 cells with stable knockdown of IMPA2 expression led to apparently reduced tumor growth in vivo ([Fig. 7C and D](#)). Additionally, we detected Ki67 by immunohistochemistry in tumor tissues from mice, showing knockdown of IMPA2 expression caused a remarkable decrease of Ki67 expression ([Supplementary Fig. S7D](#)). To explore clinical implications of IMPA2 expression for breast cancer progression, we first analyzed IMPA2 expression and its correlation with tumor size of breast cancer patients in NKI295, GSE7390 and MEBTABRIC datasets. Patients were divided into two groups according to the primary tumor size, showing that high IMPA2 expression was associated with a larger tumor size ([Fig. 7E](#)). Subsequently, we assessed the correlation of IMPA2 expression with histological grades of the tumors in NKI295, GSE25066,

and GSE22358 datasets in which tumors had the grading scores. We segregated patient into three groups according to breast cancer tumor grade. IMPA2 expression was present predominantly in Grade III tumors ([Fig. 7F](#)). These data indicate that IMPA2 functions as a critical mediator of BLBC aggressiveness.

### 3.8. Inhibition of IMPA2 suppresses metastasis of breast cancer

Because NFAT signaling was involved in cell migration and invasion, we speculated that IMPA2 expression might be critical for breast cancer metastasis. To test this notion, we first evaluated the role of IMPA2 in tumor metastasis using a xenograft metastasis model in which MDA-MB231 cells were injected via tail vein to generate pulmonary metastases. Strikingly, knockdown of IMPA2 expression suppressed lung metastasis in vivo ([Fig. 8A](#)). Next, we sought to elucidate the clinical relevance of this observation. We assessed the IMPA2 expression and its association with metastasis of breast cancer patients in GSE25066 and NKI295 datasets. Patients were divided into two groups according to their metastatic status. Tumors with high IMPA2 expression had a higher

A

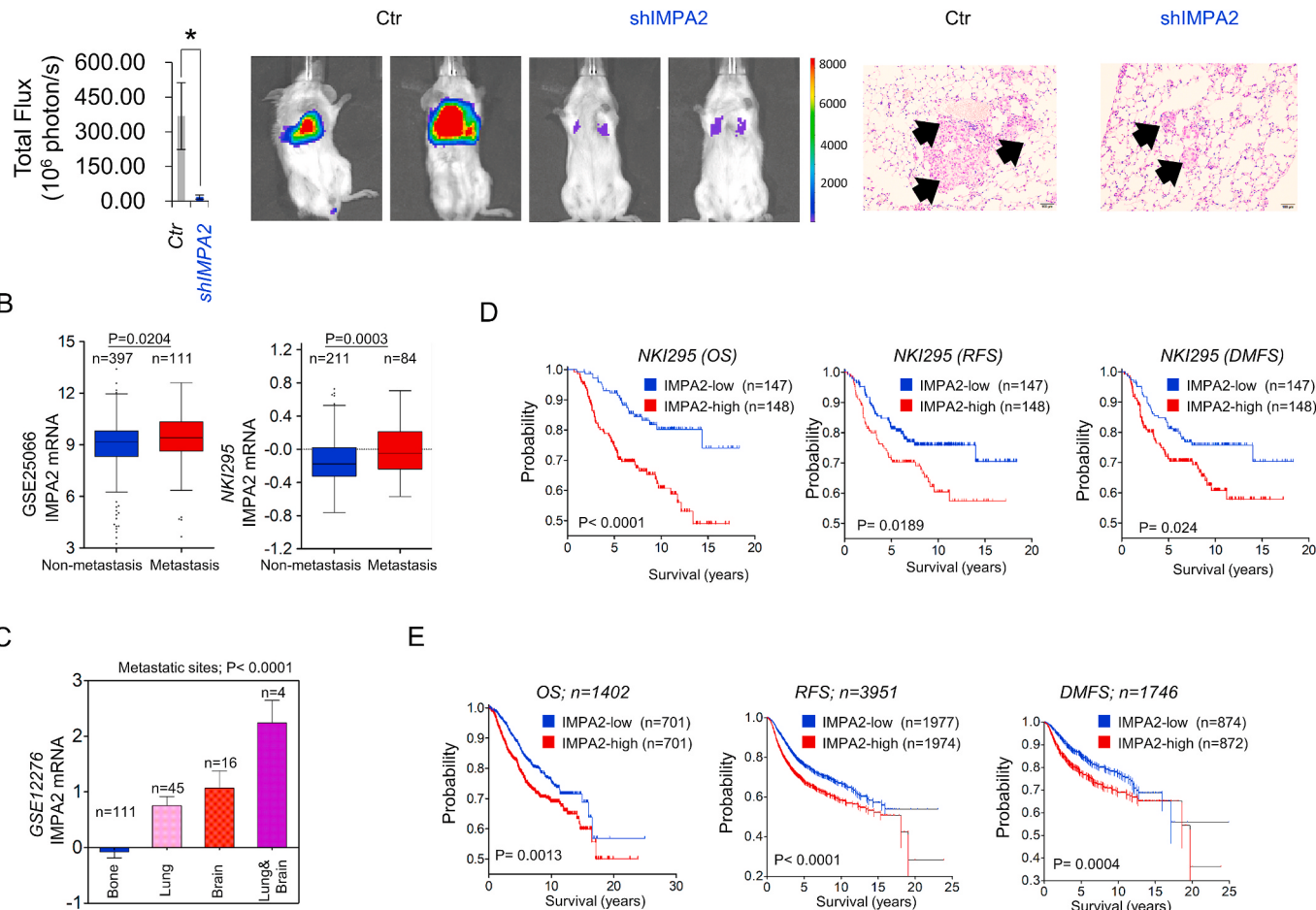


**Fig. 8.** Knockdown of IMPA2 expression suppresses metastasis in vivo, and elevated IMPA2 predicts poor clinical outcomes. (A) MDA-MB231 cells with stable empty vector or knockdown of IMPA2 expression were injected into SCID mice via the tail vein. After 4 weeks, lung metastases were quantified using bioluminescence imaging (mean of 8 mice  $\pm$  SEM) (left). Representative bioluminescence images from each group are shown (middle). The paraffin-embedded sections from lung metastatic specimens were stained with hematoxylin and eosin. Scale bar = 100  $\mu$ m (right). (B) Analysis of IMPA2 expression in breast cancer patients with or without metastasis from the GSE25066 and NKI295 dataset. (C) Analysis of the GSE12276 dataset for the association of IMPA2 expression with the metastatic tendency of primary breast tumor. (D) Kaplan-Meier survival analysis for OS, RFS, and DMFS of patients in the NKI295 dataset according to IMPA2 expression status. The p value was determined using the log-rank test. (E) Kaplan-Meier survival analysis for OS, RFS, and DMFS of patients in an aggregate breast cancer dataset according to IMPA2 expression status. The p value was determined using the log-rank test.

probability of developing metastasis than those with low IMPA2 expression (Fig. 8B). We also examined if there was a correlation between IMPA2 expression and metastatic sites in the GSE12276 dataset with 204 breast cancer patients. Consistently, primary tumors with high IMPA2 expression preferentially metastasized to the brain and lungs (Fig. 8C). These data suggest that IMPA2 plays key roles in BLBC cell metastases.

Having identified the critical function of IMPA2 in breast cancer, we performed Kaplan-Meier analyses to determine the association of IMPA2 with clinical survival by analyzing NKI295 datasets. Patients were divided into two groups based upon IMPA2 expression levels. Survival analysis demonstrated that patients with high IMPA2 expression exhibited shorter overall survival (OS), relapse-free survival (RFS), and distant metastasis free survival (DMFS) (Fig. 8D). In addition, we used an aggregate breast cancer dataset to determine its clinical relevance, showing that tumors with high IMPA2 expression had shorter OS, RFS, and DMFS (Fig. 8E). These clinical data support the critical role of IMPA2 in breast cancer aggressiveness.

#### 4. Discussion

In this study, we report that inhibition of IMPA2 suppresses the tumorigenic and metastatic activities and elucidate the underlying mechanisms. Our study provides several new insights into the critical roles of IMPA2 in BLBC.

##### 4.1. IMPA2 copy number amplification, hypomethylation of IMPA2 promoter and MYC-mediated transcriptional activation contribute to elevated IMPA2 expression in BLBC

CNVs play key roles in many types of cancer. Several CNVs that are correlated with poor outcomes have been studied in BLBC [44,45]. Our study also demonstrated that IMPA2 overexpression was partially due to the copy number amplification. CNV is a critical factor that regulates mRNA expression. In this study, we showed that cases with copy number amplification of IMPA2 had a significantly higher IMPA2 expression than those with no amplification by analyzing copy number variations in different subtypes of breast cancer tissues and cell lines from TCGA, METABRIC and CCLE datasets. In addition, cases with IMPA2 copy number amplification were associated with BLBC subtype. These results

suggest that IMPA2 copy number amplification is positively correlated with IMPA2 expression and BLBC.

Some breast tumors with IMPA2 overexpression were observed to have no copy number amplification of IMPA2, indicating the involvement of other factors in regulating IMPA2 expression. DNA hypermethylation causes gene silencing by preventing the binding of transcription factors to their recognition sequence, whereas DNA hypomethylation is related to gene activation by reversing this binding suppression [46,47]. Our data showed that low methylation in the promoter of IMPA2 was correlated with high expression of IMPA2 and BLBC through analyzing IMPA2 methylation and gene expression datasets, indicating that IMPA2 promoter hypomethylation is another critical reason for IMPA2 overexpression in BLBC.

MYC as a key transcriptional activator controlling cell metabolism, proliferation, migration and metastasis [48,49]. MYC is frequently overexpressed in BLBC, playing key roles in tumor recurrence, metastasis, and chemotherapy response [50,51]. Correlation analysis in large breast cancer gene expression datasets demonstrated a positive correlation between IMPA2 and MYC expression. Ectopic expression of MYC in breast cancer cells significantly promoted IMPA2 expression. In addition, ChIP and ChIP-seq analysis showed that MYC was highly enriched in the promoter of IMPA2 in multiple cells. Together, our data identified that MYC is a direct transcriptional activator responsible for high IMPA2 expression in BLBC.

#### 4.2. IMPA2 expression facilitates BLBC aggressiveness by a MYC-mediated positive feedback loop

In this study, we found that IMPA2 expression was especially elevated in BLBC, and BLBC had significantly elevated MI level due to IMPA2 expression. In neuropsychiatric diseases, inositol monophosphates family, including IMPA1 and IMPA2, can regulate IP3/Ca<sup>2+</sup> signaling by changing MI-PI cycle [8,13–15]. The altered IP3/Ca<sup>2+</sup> signaling is associated with tumor proliferation, migration, invasion, and metastasis [8,52]. The IP3Rs consist of three isoforms: IP3R1, IP3R2, and IP3R3. IP3 activates Ca<sup>2+</sup> signaling by binding IP3Rs. IP3R, especially IP3R3, promotes breast cancer cell proliferation [16] and migration [18,19], suggesting a crucial role of IP3/Ca<sup>2+</sup> signaling in breast cancer. Our data showed that knockdown of IMPA2 expression decreased MI, IP3 level and Ca<sup>2+</sup> concentration in breast cancer cells, indicating that IMPA2 expression enhances BLBC aggressiveness by activating IP3/Ca<sup>2+</sup> signaling.

Ca<sup>2+</sup> signaling functions in cancer cells through upregulating oncogenes and/or downregulating tumor suppressors. In cell, NFAT is a Ca<sup>2+</sup> sensor. Ca<sup>2+</sup> changes can induce the activation of calmodulin and calcineurin. Calcineurin then dephosphorylates multiple phosphoserines in the regulatory domain, leading to the nuclear translocation of NFAT. In the nucleus, NFAT cooperates with multiple transcriptional partners to initiate and maintain specific gene expressions [39,40]. Importantly, NFAT1 is constitutively activated in triple-negative breast cancer and promotes tumorigenesis and metastasis [53,54]. Our study showed that knockdown of IMPA2 expression decreased the Ca<sup>2+</sup> concentration and inhibited NFAT1 translocation to the nucleus, supporting the key role of IMPA2-mediated Ca<sup>2+</sup>-NFAT1 axis in the aggressive behavior of BLBC. Interestingly, NFAT1 can directly bind to a specific element within the proximal MYC promoter and upregulates MYC transcription [39–41].

Together, MYC can transcriptionally promote IMPA2 expression, activating Ca<sup>2+</sup>-NFAT1 axis, whereas NFAT1 directly upregulates MYC transcription, thus fulfilling a positive feedback loop that enhances tumorigenicity and metastasis of BLBC cells (Fig. 6H).

#### 4.3. IMPA2 represents a potential prognostic indicator and therapeutic target for BLBC

We have shown IMPA2 expression is associated with several factors that predict the risk of cancer progression and patient prognosis,

including [1] Breast cancer subtypes: IMPA2 expression is especially elevated in BLBC [2]; Grade: high IMPA2 expression is associated with patients with higher grade tumors [3]; Tumor size: high IMPA2 expression is significantly correlated with larger tumor size [4]; Tumor metastasis: high IMPA2 expression is positively correlated with metastasis and metastatic dissemination to the brain and lungs, which is line with the metastatic tendency of BLBC [5]; Survival rate: high IMPA2 expression predicts poor overall, relapse-free, and distant metastasis-free survival. These findings strongly support that IMPA2 is a promising prognostic biomarker for breast cancer patients.

Owing to the lack of effective targeted agents and poor response to standard chemotherapy, identification of novel molecular targets in BLBC is urgently needed. In this study, IMPA2 overexpression represents an oncogenic event that associates with BLBC aggressiveness, and inhibition of IMPA2 by small molecules may provide an attractive new approach for the clinical treatment of BLBC. Lithium, a mood stabilizer drug used to treat bipolar disorder, had been identified as an inhibitor for inositol monophosphatase protein family [55]. In our study, we also tested the effect of lithium on breast cancer cells. Consistent with previous researches, we found that lithium had minimal inhibitory effects on IMPA2 activity, and cancer cell migration and invasion at physiological concentrations (data not shown), and thus developing effective IMPA2 inhibitors might be promising targeted drugs for treating BLBC.

#### Ethics approval and consent to participate

The experiments were performed according to the approved guidelines established by the institutional review board at Zhejiang University, Hangzhou, China. Animal experiments were performed according to procedures approved by the Institutional Animal Care and Use Committee at the Zhejiang University, Hangzhou, China.

#### Consent for publication

Not applicable.

#### Availability of data and materials

The microarray datasets that were utilized in the study were retrieved from the NIH-GEO dataset database (<http://www.ncbi.nlm.nih.gov/gds/>), EMBL-EBI dataset database (<https://www.ebi.ac.uk/>) and Cancer Cell Line Encyclopedia (<https://sites.broadinstitute.org/cclle>). Information about TCGA and the investigators and institutions that constitute the TCGA research network can be found at <http://cancergenome.nih.gov/>. Other data generated during this study are included in this published article.

#### Funding

This work was supported by grants from Natural Science Foundation of China (No. 82372815, 82173112, and 81972456 to C.D.; No. 82373281 to Z.D.; No. 82103350 to Q.C.; No. 32200619 to X.C.), Natural Science Foundation of Jiangxi Province (No. 20232BAB206093 to X.W.) and Key Project of Zhejiang Natural Science Foundation (No. Z22H169268 to Z.D.).

#### CRediT authorship contribution statement

**Xingyu Lei:** Writing – review & editing, Writing – original draft, Validation, Resources, Data curation, Conceptualization. **Ruocen Liao:** Validation, Conceptualization. **Xingyu Chen:** Funding acquisition, Data curation. **Zhenzhen Wang:** Data curation. **Qianhua Cao:** Data curation. **Longchang Bai:** Data curation. **Chenglong Ma:** Data curation. **Xinyue Deng:** Conceptualization. **Yihua Ma:** Data curation. **Xuebiao Wu:** Data curation. **Jun Li:** Writing – review & editing. **Zhijun Dai:** Writing – review & editing. **Chenfang Dong:** Writing – review & editing, Writing –

original draft, Resources, Funding acquisition, Conceptualization.

## Declaration of competing interest

The authors declare that they have no known competing financial interests or personal relationships that could have appeared to influence the work reported in this paper.

## Acknowledgements

Not applicable.

## Appendix A. Supplementary data

Supplementary data to this article can be found online at <https://doi.org/10.1016/j.canlet.2023.216527>.

## References

- [1] E.A. Rakha, J.S. Reis-Filho, I.O. Ellis, Basal-like breast cancer: a critical review, *J. Clin. Oncol. : Offic. J. Am. Soc. Clin. Oncol.* 26 (15) (2008) 2568–2581.
- [2] B. Kreike, M. van Kouwenhove, H. Horlings, B. Weigelt, H. Peterse, H. Bartelink, et al., Gene expression profiling and histopathological characterization of triple-negative/basal-like breast carcinomas, *Breast Cancer Res.* 9 (5) (2007) R65.
- [3] O. Fadare, F.A. Tavassoli, Clinical and pathologic aspects of basal-like breast cancers, *Nat. Clin. Pract. Oncol.* 5 (3) (2008) 149–159.
- [4] R. Dent, M. Trudeau, K.I. Pritchard, W.M. Hanna, H.K. Kahn, C.A. Sawka, et al., Triple-negative breast cancer: clinical features and patterns of recurrence, *Clin. Cancer Res. : Offic. J. Am. Assoc. Cancer Res.* 13 (15 Pt 1) (2007) 4429–4434.
- [5] A. Bergamaschi, G.O. Hjortland, T. Trulzeti, T. Sørlie, H. Johnsen, A.H. Ree, et al., Molecular profiling and characterization of luminal-like and basal-like *in vivo* breast cancer xenograft models, *Mol. Oncol.* 3 (5–6) (2009) 469–482.
- [6] D. Hanahan, R.A. Weinberg, Hallmarks of cancer: the next generation, *Cell* 144 (5) (2011) 646–674.
- [7] M.L. Croze, C.O. Soulage, Potential role and therapeutic interests of myo-inositol in metabolic diseases, *Biochimie* 95 (10) (2013) 1811–1827.
- [8] M.J. Berridge, The inositol trisphosphate/calcium signaling pathway in health and disease, *Physiol. Rev.* 96 (4) (2016) 1261–1296.
- [9] T. Balla, Phosphoinositides: tiny lipids with giant impact on cell regulation, *Physiol. Rev.* 93 (3) (2013) 1019–1137.
- [10] L.M. Thorpe, H. Yuzugullu, J.J. Zhao, PI3K in cancer: divergent roles of isoforms, modes of activation and therapeutic targeting, *Nat. Rev. Cancer* 15 (1) (2015) 7–24.
- [11] I. Vucenik, A.M. Shamsuddin, Cancer inhibition by inositol hexaphosphate (IP6) and inositol: from laboratory to clinic, *J. Nutr.* 133 (11 Suppl 1) (2003), 3778s–84s.
- [12] K.C. Case, M.W. Schmidtke, M.L. Greenberg, The paradoxical role of inositol in cancer: a consequence of the metabolic state of a tumor, *Cancer Metastasis Rev.* 41 (2) (2022) 249–254.
- [13] S. Sarkar, D.C. Rubinsztein, Inositol and IP3 levels regulate autophagy: biology and therapeutic speculations, *Autophagy* 2 (2) (2006) 132–134.
- [14] S. Sarkar, G. Krishna, S. Imarisio, S. Saiki, C.J. O’Kane, D.C. Rubinsztein, A rational mechanism for combination treatment of Huntington’s disease using lithium and rapamycin, *Hum. Mol. Genet.* 17 (2) (2008) 170–178.
- [15] S. Sarkar, R.A. Floto, Z. Berger, S. Imarisio, A. Cordenier, M. Pasco, et al., Lithium induces autophagy by inhibiting inositol monophosphatase, *J. Cell Biol.* 170 (7) (2005) 1101–1111.
- [16] A. Mound, L. Rodat-Despoix, S. Bougarn, H. Ouadid-Ahidouch, F. Matifat, Molecular interaction and functional coupling between type 3 inositol 1,4,5-trisphosphate receptor and BKCa channel stimulate breast cancer cell proliferation, *Eur. J. Cancer* 49 (17) (2013) 3738–3751. Oxford, England : 1990.
- [17] A. Singh, M. Chagtoo, S. Tiwari, N. George, B. Chakravarti, S. Khan, et al., Inhibition of inositol 1, 4, 5-trisphosphate receptor induce breast cancer cell death through deregulated autophagy and cellular bioenergetics, *J. Cell. Biochem.* 118 (8) (2017) 2333–2346.
- [18] A. Vautrin-Glabik, B. Botia, P. Kischel, H. Ouadid-Ahidouch, Rodat-Despoix L. IP(3)R3 silencing induced actin cytoskeletal reorganization through ARHGAP18/RhoA/mDia1/FAK pathway in breast cancer cell lines, *Biochim. Biophys. Acta Mol. Cell Res.* 1865 (7) (2018) 945–958.
- [19] A. Mound, A. Vautrin-Glabik, A. Foulon, B. Botia, F. Hague, J.B. Parys, et al., Downregulation of type 3 inositol (1,4,5)-trisphosphate receptor decreases breast cancer cell migration through an oscillatory Ca2+ signal, *Oncotarget* 8 (42) (2017) 72324–72341.
- [20] C. Dong, Y. Wu, J. Yao, Y. Wang, Y. Yu, P.G. Rychahou, et al., G9a interacts with Snail and is critical for Snail-mediated E-cadherin repression in human breast cancer, *J. Clin. Invest.* 122 (4) (2012) 1469–1486.
- [21] Y. Lin, Y. Wu, J. Li, C. Dong, X. Ye, Y.I. Chi, et al., The SNAG domain of Snail functions as a molecular hook for recruiting lysine-specific demethylase 1, *EMBO J.* 29 (11) (2010) 1803–1816.
- [22] C. Dong, T. Yuan, Y. Wu, Y. Wang, T.W. Fan, S. Miriyala, et al., Loss of FBP1 by Snail-mediated repression provides metabolic advantages in basal-like breast cancer, *Cancer Cell* 23 (3) (2013) 316–331.
- [23] X. Wu, X. Li, Q. Fu, Q. Cao, X. Chen, M. Wang, et al., AKR1B1 promotes basal-like breast cancer progression by a positive feedback loop that activates the EMT program, *J. Exp. Med.* 214 (4) (2017) 1065–1079.
- [24] Q. Cao, X. Chen, X. Wu, R. Liao, P. Huang, Y. Tan, et al., Inhibition of UGT8 suppresses basal-like breast cancer progression by attenuating sulfatide-αVβ5 axis, *J. Exp. Med.* 215 (6) (2018) 1679–1692.
- [25] Z. Miao, Q. Cao, R. Liao, X. Chen, X. Li, L. Bai, et al., Elevated transcription and glycosylation of B3GNT5 promotes breast cancer aggressiveness, *J. Exp. Clin. Cancer Res. : CR* 41 (1) (2022) 169.
- [26] P. Huang, R. Liao, X. Chen, X. Wu, X. Li, Y. Wang, et al., Nuclear translocation of PLSCR1 activates STAT1 signaling in basal-like breast cancer, *Theranostics* 10 (10) (2020) 4644–4658.
- [27] X. Chen, Q. Cao, R. Liao, X. Wu, S. Xun, J. Huang, et al., Loss of ABAT-mediated GABAergic system promotes basal-like breast cancer progression by activating Ca (2+)-NFAT1 Axis, *Theranostics* 9 (1) (2019) 34–47.
- [28] Y. Pawitan, J. Bjökhle, L. Amler, A.L. Borg, S. Eggerz, P. Hall, et al., Gene expression profiling spares early breast cancer patients from adjuvant therapy: derived and validated in two population-based cohorts, *Breast Cancer Res.* 7 (6) (2005) R953–R964.
- [29] C. Hatzis, L. Pusztai, V. Valero, D.J. Booser, L. Esserman, A. Lluch, et al., A genomic predictor of response and survival following taxane-anthracycline chemotherapy for invasive breast cancer, *JAMA* 305 (18) (2011) 1873–1881.
- [30] M.J. van de Vijver, Y.D. He, L.J. van’t Veer, H. Dai, A.A. Hart, D.W. Voskuil, et al., A gene-expression signature as a predictor of survival in breast cancer, *N. Engl. J. Med.* 347 (25) (2002) 1999–2009.
- [31] P. Mertins, D.R. Mani, K.V. Ruggles, M.A. Gillette, K.R. Clouser, P. Wang, et al., Proteogenomics connects somatic mutations to signalling in breast cancer, *Nature* 534 (7605) (2016) 55–62.
- [32] K.P. Hoeflich, C. O’Brien, Z. Boyd, G. Cavet, S. Guerrero, K. Jung, et al., In vivo antitumor activity of MEK and phosphatidylinositol 3-kinase inhibitors in basal-like breast cancer models, *Clin. Cancer Res. : Offic. J. Am. Assoc. Cancer Res.* 15 (14) (2009) 4649–4664.
- [33] L.M. Heiser, A. Sadanandam, W.L. Kuo, S.C. Benz, T.C. Goldstein, S. Ng, et al., Subtype and pathway specific responses to anticancer compounds in breast cancer, *Proc. Natl. Acad. Sci. U.S.A.* 109 (8) (2012) 2724–2729.
- [34] M. Pariyar, A. Johns, R.F. Thorne, R.J. Scott, K.A. Avery-Kiejda, Copy number variation in triple negative breast cancer samples associated with lymph node metastasis, *Neoplasia* 23 (8) (2021) 743–753.
- [35] H. Zhu, G. Wang, J. Qian, Transcription factors as readers and effectors of DNA methylation, *Nat. Rev. Genet.* 17 (9) (2016) 551–565.
- [36] X. Tang, C.C. Lin, I. Spasojevic, E.S. Iversen, J.T. Chi, J.R. Marks, A joint analysis of metabolomics and genetics of breast cancer, *Breast Cancer Res.* 16 (4) (2014) 415.
- [37] S. Dubuis, F. Baenke, N. Scherbichler, L.T. Alexander, A. Schulze, N. Zamboni, Metabotypes of breast cancer cell lines revealed by non-targeted metabolomics, *Metab. Eng.* 43 (Pt B) (2017) 173–186.
- [38] T. Ohnishi, H. Ohba, K.C. Seo, J. Im, Y. Sato, Y. Iwayama, et al., Spatial expression patterns and biochemical properties distinguish a second myo-inositol monophosphatase IMPA2 from IMPA1, *J. Biol. Chem.* 282 (1) (2007) 637–646.
- [39] M.R. Müller, A. Rao, NFAT, immunity and cancer: a transcription factor comes of age, *Nat. Rev. Immunol.* 10 (9) (2010) 645–656.
- [40] M. Mancini, A. Toker, NFAT proteins: emerging roles in cancer progression, *Nat. Rev. Cancer* 9 (11) (2009) 810–820.
- [41] M. Buchholz, A. Schatz, M. Wagner, P. Michl, T. Linhart, G. Adler, et al., Overexpression of c-myc in pancreatic cancer caused by ectopic activation of NFATc1 and the Ca2+/calcineurin signaling pathway, *EMBO J.* 25 (15) (2006) 3714–3724.
- [42] B.C. Jiang, T.Y. Ding, C.Y. Guo, X.H. Bai, D.L. Cao, X.B. Wu, et al., NFAT1 orchestrates spinal microglial transcription and promotes microglial proliferation via c-MYC contributing to nerve injury-induced neuropathic pain, *Adv. Sci.* 9 (27) (2022), e2201300.
- [43] G. Singh, S.K. Singh, A. König, K. Reutlinger, M.D. Nye, T. Adhikary, et al., Sequential activation of NFAT and c-Myc transcription factors mediates the TGF-β beta switch from a suppressor to a promoter of cancer cell proliferation, *J. Biol. Chem.* 285 (35) (2010) 27241–27250.
- [44] X. Pan, X. Hu, Y.H. Zhang, L. Chen, L. Zhu, S. Wan, et al., Identification of the copy number variant biomarkers for breast cancer subtypes, *Mol. Genet. Genom. : MG* 294 (1) (2019) 95–110.
- [45] P. Concolino, R. Rizza, F. Mignone, A. Costella, D. Guarino, I. Carboni, et al., A comprehensive BRCA1/2 NGS pipeline for an immediate Copy Number Variation (CNV) detection in breast and ovarian cancer molecular diagnosis, *Clinica chimica acta*; *Int. J. Clin. Chem.* 480 (2018) 173–179.
- [46] K. Skvortsova, E. Masle-Farquhar, P.L. Luu, J.Z. Song, W. Qu, E. Zotenko, et al., DNA hypermethylation encroachment at CpG island borders in cancer is predisposed by H3K4 monomethylation patterns, *Cancer Cell* 35 (2) (2019) 297–314.e8.
- [47] A. Eden, F. Gaudet, A. Waghmare, R. Jaenisch, Chromosomal instability and tumors promoted by DNA hypomethylation, *Science* 300 (5618) (2003) 455.
- [48] D.M. Miller, S.D. Thomas, A. Islam, D. Muench, K. Sedoris, c-Myc and cancer metabolism, *Clin. Cancer Res. : Offic. J. Am. Assoc. Cancer Res.* 18 (20) (2012) 5544–5553.
- [49] C.V. Dang, MYC on the path to cancer, *Cell* 149 (1) (2012) 22–35.
- [50] Comprehensive molecular portraits of human breast tumours, *Nature* 490 (7418) (2012) 61–70.

- [51] D. Horiuchi, L. Kusdra, N.E. Huskey, S. Chandriani, M.E. Lenburg, A.M. Gonzalez-Angulo, et al., MYC pathway activation in triple-negative breast cancer is synthetic lethal with CDK inhibition, *J. Exp. Med.* 209 (4) (2012) 679–696.
- [52] G.R. Monteith, D. McAndrew, H.M. Faddy, S.J. Roberts-Thomson, Calcium and cancer: targeting Ca<sup>2+</sup> transport, *Nat. Rev. Cancer* 7 (7) (2007) 519–530.
- [53] C.T. Quang, S. Leboucher, D. Passaro, L. Fuhrmann, M. Nourieh, A. Vincent-Salomon, et al., The calcineurin/NFAT pathway is activated in diagnostic breast cancer cases and is essential to survival and metastasis of mammary cancer cells, *Cell Death Dis.* 6 (2) (2015) e1658.
- [54] J.J. Qin, W. Wang, R. Zhang, Experimental therapy of advanced breast cancer: targeting NFAT1-MDM2-p53 pathway, *Progress Molecul. Biol. Translat. Sci.* 151 (2017) 195–216.
- [55] A. Can, T.G. Schulze, T.D. Gould, Molecular actions and clinical pharmacogenetics of lithium therapy, *Pharmacol. Biochem. Behav.* 123 (2014) 3–16.